

Analysis of Collaborative Beamforming Designs in Real-World Environments

Slim Zaidi and Sofiène Affes

INRS-EMT, 800, de la Gauchetière Ouest, Bureau 6900, Montréal, H5A 1K6, Qc, Canada.

Abstract—Three main collaborative beamforming (CB) designs based on different channel models could be applied in real-world environments where local scattering and implementation imperfections might exist: the optimal CSI-based CB (OCB), the conventional or monochromatic (i.e., single-ray) distributed CB (M-DCB), and the recently developed bichromatic (i.e., two-ray) distributed CB (B-DCB). In this paper, we perform an analytical comparison, under practical constraints, between these CB designs in terms of achieved signal-to-noise ratio (SNR) as well as achieved throughput. Assuming the presence of local scattering in the source vicinity and accounting for implementation errors incurred by each CB design, we derive for the first time closed-form expressions of their true achieved SNRs. At a low angular spread (AS) where both designs nominally achieve the same SNR in ideal conditions, we show that the B-DCB always outperforms OCB, more so and at larger regions of AS values when errors increase. Excluding exceptional circumstances of unrealistic low quantization levels (i.e., very large quantization errors) hard to justify in practice, we also show that the new B-DCB always outperforms the M-DCB as recently found nominally in ideal conditions. This work is also the first to push the performance analysis of CB to the throughput level by taking into account the feedback overhead cost incurred by each design. We prove both by concordant analysis and simulations that the B-DCB is able to outperform, even for high AS values, the OCB which is penalized by its prohibitive implementation overhead, especially for a large number of collaborating terminals and/or high Doppler frequencies.

I. INTRODUCTION AND BACKGROUND

Collaborative beamforming (CB) is a strong means to establish energy-efficient and reliable communications over long distances [1]-[4]. Despite of its practical merits, CB faces an important issue. Indeed, the collaborating terminals are very often autonomous small battery-powered units which have limited knowledge about each other in the network. In the very likely event where the beamforming weights would depend on the locally unavailable information at every terminal, the latter would not be able to compute its own weight without severely depleting power and bandwidth due to the potentially huge information exchange requested [3]. Lending themselves to a distributed implementation, a variety of so-called distributed CB (DCB) techniques wherein the designed weights solely depend on the information commonly available at every terminal and, hence, each terminal is able to locally compute its own weight were proposed in [3] and

[4]. So far, however, such works neglected the scattering and reflection effects and assumed plane-wave (single-ray) propagation channels termed here as monochromatic (with reference to their angular distribution). This assumption is not valid in real-world environments where the presence of local scattering in the source vicinity causes an angular spread (AS) of the transmit signal that forms a multi-ray propagation channel [5]-[7]. Due to the resulting mismatch between the nominal single-ray and the true multi-ray channels, it was shown in [6] that the performance of monochromatic DCB (M-DCB) techniques degrades in rural areas where the AS is still very small and becomes unsatisfactory when the AS increases such as in suburban and urban areas. This impediment unfortunately limits the DCB's real-world applicability range. It is noteworthy that the well-known CSI-based CB design could properly handle real-world environments, but the overhead associated with the channel estimations would be prohibitive, especially when the number of collaborating terminals is large and/or when estimates have to be frequently updated at high Doppler [8], [9]. In [10] and [11], we have recently developed a new CB design that combines the benefits of M-DCB (i.e., small-overhead distributed implementation) and OCB (i.e., better match with true channel in scattered environments) and which avoids their respective drawbacks (channel mismatch and large overhead).

In this work, we consider for analysis not only the M-DCB and the B-DCB but also the optimal CSI-based CB (OCB) design. Assuming the presence of local scattering in the source vicinity and accounting for estimation and quantization errors incurred by each CB design, we compare their achieved SNRs in practical conditions. To this end, we derive for the first time their true achieved SNRs in closed-form taking into account estimation and feedback quantization errors. For low AS, where both designs nominally achieve the same SNR in ideal conditions, we show that the B-DCB always outperforms OCB, more so and at larger regions of AS values when errors increase. Excluding exceptional circumstances of unrealistic low quantization levels (i.e., very large quantization errors) hard to justify in practice, we also show that the new B-DCB always outperforms the M-DCB as recently found nominally in ideal conditions. This work is also the first to push the performance analysis of CB to the throughput level by taking into account the feedback overhead cost incurred by each design. We prove both by concordant analysis and simulations that the B-DCB is able to outperform, even for high AS values,

Work supported by a Canada Research Chair in Wireless Communications and the Discovery Grants Program of NSERC.

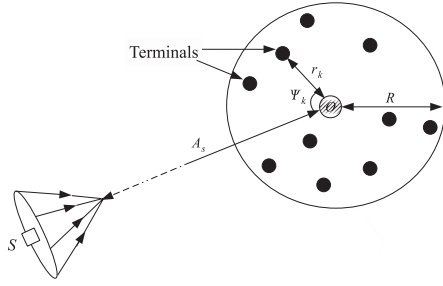


Fig. 1. System model.

the OCB which is penalized by its prohibitive implementation overhead, especially for a large number of collaborating terminals and/or high Doppler frequencies. Indeed, it is shown that the operational regions in terms of AS values over which the new B-DCB is favored against OCB in terms of achieved throughput can reach up to 40 deg.

The rest of this paper is organized as follows. The system model is described in Section II. The CB techniques in the presence of local scattering are presented in Section III. Section IV compares the performance of these techniques in terms of ASANR while Section V compares them in terms of the link-level throughput. Simulations results are shown in Section VI and concluding remarks are given in Section VII.

Notation: Uppercase and lowercase bold letters denote matrices and vectors, respectively. $[\cdot]_{il}$ and $[\cdot]_i$ are the (i, l) -th entry of a matrix and i -th entry of a vector, respectively. $(\cdot)^T$ and $(\cdot)^H$ denote the transpose and the Hermitian transpose, respectively. $J_1(\cdot)$ is the first-order Bessel function of the first kind.

II. SYSTEM MODEL

As illustrated in Fig. 1, the system of interest consists of a wireless network or subnetwork comprised of K uniformly and independently distributed terminals on $D(O, R)$, the disc with center at O and radius R , a receiver at O , and a source S located in the same plane containing $D(O, R)$ [1], [2]. We assume that there is no direct link from the source to the receiver due to pathloss attenuation. Moreover, let (r_k, ψ_k) denote the polar coordinates of the k -th terminal and (A_s, ϕ_s) denote those of the source. The latter is assumed to be at $\phi_s = 0$, without loss of the generality, and to be located in the far-field region, hence, $A_s \gg R$.

The following assumptions are further considered:

A1) The far-field source is scattered by a large number of scatterers within its vicinity. The latters generate from the transmit signal L equal-power rays or "spatial chromatics" (with reference to their angular distribution) that form an L -ray propagation channel [5]-[7]. The l -th ray or chromatic is characterized by its angle θ_l and its complex amplitude $\alpha_l = \rho_l e^{j\xi_l}$ where the amplitudes ρ_l , $l = 1, \dots, L$ and the phases ξ_l , $l = 1, \dots, L$ are independent and identically distributed (i.i.d.) random variables, and each phase is uniformly distributed over $[-\pi, \pi]$. The θ_l , $l = 1, \dots, L$ are also i.i.d. random variables with variance σ_θ^2 and probability density function (pdf) $p(\theta)$ [5]-[7]. All θ_l s, ξ_l s, and ρ_l s are mutually

independent. Note that the standard deviation σ_θ is commonly known as the angular spread (AS) while $p(\theta)$ is called the scattering or angular distribution.

A2) The channel gain $[\mathbf{f}]_k$ between the k -th terminal and the receiver is a zero-mean unit-variance circular Gaussian random variable [3]. The source signal s is a zero-mean random variable with unit-power while noises at terminals and the receiver are zero-mean Gaussian random variables with variances σ_v^2 and σ_n^2 , respectively. The source signal, noises, and the terminals forward or backward channel gains are mutually independent [3].

A4) The k -th terminal is aware of its own coordinates (r_k, ψ_k) , its forward channel $[\mathbf{f}]_k$, the directions of the source ϕ_s , K , and σ_θ^2 while being oblivious to the locations and the forward and backward channels of *all* other terminals in the network.

Using A1 and the fact that $A_s \gg R$, the channel gain between the k -th terminal and the source or the receiver, respectively, can be represented as $[\mathbf{g}]_k = \sum_{l=1}^L \alpha_l e^{-j\frac{2\pi}{\lambda} r_k \cos(\theta_l - \psi_k)}$ where λ is the wavelength.

III. CB TECHNIQUES IN THE PRESENCE OF LOCAL SCATTERING

A dua-hop communication is established from the source S to the receiver. In the first time slot, the source sends its signal s to the wireless network while in the second time slot, the k -th terminal multiplies its received signal with the complex conjugate of the beamforming weight w_k and forwards the resulting signal to the receiver. Several approaches can be adopted to properly select the beamforming weights. In this paper, we are only concerned with the approach that aims to minimize the noise power while fixing the beamforming response in the desired direction equal to 1. Based on different channel models several beamforming designs exist in the literature to perform these tasks. If \mathbf{w}_* denotes the beamforming vector associated with one of these designs, it is then the solution of the following optimization problem [3]:

$$\mathbf{w}_* = \arg \min \mathbf{w}^H \mathbf{\Lambda} \mathbf{w} \quad \text{s.t.} \quad \mathbf{w}^H \mathbf{h}_* = 1, \quad (1)$$

where $\mathbf{\Lambda} \triangleq \text{diag}\{[|\mathbf{f}]_1|^2 \dots [|\mathbf{f}]_K|^2\}$. It can be readily proven that \mathbf{w}_* is given by

$$\mathbf{w}_* = \mu_* \mathbf{\Lambda}^{-1} \mathbf{h}_*. \quad (2)$$

where μ_* is the factor chosen such that the constraint in (1) is satisfied. In the sequel, we will explore the main existing beamforming designs and compare their performances.

1) *Optimal CB (OCB):* The optimal CB (OCB) is the well known CSI-based design and, hence, its beamforming vector is given by [8], [9]

$$\mathbf{w}_O = \mu_O \mathbf{\Lambda}^{-1} \mathbf{h}_O \quad (3)$$

where $\mathbf{h}_O = \mathbf{h}$ and $\mu_O = (\mathbf{h}_O^H \mathbf{\Lambda}^{-1} \mathbf{h}_O)^{-1}$. From (3), in order to implement the OCB technique, the source must estimate and quantize the channels $[\mathbf{h}]_k$, $k = 1 \dots K$ before sending them back to all K terminals. This process unfortunately results in

both estimation and quantization errors as well as an important overhead. Let us denote the resulting channel vector by $\hat{\mathbf{h}}_O = \mathbf{h}_O + \mathbf{e}_O$ where $\mathbf{e}_O = \mathbf{f} \odot \mathbf{e}_c + \mathbf{f} \odot \mathbf{e}_{cq}$ and \mathbf{e}_c and \mathbf{e}_{cq} are the channel identification and quantization errors, respectively. Let us denote the variance of \mathbf{e}_O by $\sigma_{\mathbf{e}_O}^2 = \sigma_{\mathbf{e}_c}^2 + \sigma_{\mathbf{e}_{cq}}^2$ where $\sigma_{\mathbf{e}_c}^2$ and $\sigma_{\mathbf{e}_{cq}}^2$ are the variances of \mathbf{e}_c and \mathbf{e}_{cq} , respectively. We can show that $\sigma_{\mathbf{e}_c}^2 = \frac{3K}{2} (\pi \sigma_v^2 \bar{f}_D)^{\frac{2}{3}}$ where \bar{f}_D is the normalized Doppler frequency [12]. Moreover, assuming a $(B_c + 1)$ -bit uniform quantization we have $\sigma_{\mathbf{e}_{cq}}^2 = 2^{-2B_c} \frac{h_{\text{Max}}^2}{12}$ where h_{Max} is the peak amplitude of all channels' realizations $[\mathbf{h}]_k$ for $k = 1, \dots, K$ [13]. Taking into account these considerations, the OCB's beamforming vector is now given by

$$\hat{\mathbf{w}}_O = \hat{\mu}_O \mathbf{\Lambda}^{-1} \hat{\mathbf{h}}_O \quad (4)$$

where $\hat{\mu}_O = \left(\hat{\mathbf{h}}_O^H \mathbf{\Lambda}^{-1} \hat{\mathbf{h}}_O \right)^{-1}$.

2) *Monochromatic DCB (M-DCB)*: Alternatively, when designing the CB, we could intentionally neglect the local scattering effect (i.e., assume that $\sigma_\theta \rightarrow 0$) to nominally assume a monochromatic single-ray propagation channels and, hence, the beamforming vector associated with the monochromatic DCB (M-DCB) is given by [1]

$$\mathbf{w}_M = \mu_M \mathbf{\Lambda}^{-1} \mathbf{h}_M, \quad (5)$$

where $\mathbf{h}_M = \mathbf{a}(0)$ with $[\mathbf{a}(\theta)]_k = [\mathbf{f}]_k e^{-j(2\pi/\lambda)r_k \cos(\theta + \phi_s - \psi_k)}$ and $\mu_M = \left(\mathbf{a}(0)^H \mathbf{\Lambda}^{-1} \mathbf{a}(0) \right)^{-1} = 1/K$. Also known as conventional DCB, this beamformer implementation requires that the source estimates, quantizes and sends only its direction ϕ_s [1]. This process results in both localization and quantization errors and, hence, the channel \mathbf{h}_M should be substituted by $\hat{\mathbf{h}}_M = \mathbf{h}_M e^{-j(\mathbf{e}_a + \mathbf{e}_{aq})}$ where \mathbf{e}_a and \mathbf{e}_{aq} are the angle localization and quantization errors, respectively. Assuming that these errors are relatively small and using Taylor's series series expansion, one can easily prove that $\hat{\mathbf{h}}_M \simeq \mathbf{h}_M + \mathbf{e}_M$ where $\mathbf{e}_M = -j\mathbf{h}_M (\mathbf{e}_a + \mathbf{e}_{aq})$ with variance $\sigma_{\mathbf{e}_M}^2 = \sigma_{\mathbf{e}_a}^2 + \sigma_{\mathbf{e}_{aq}}^2$. Using a $(B_a + 1)$ -bit uniform quantization, it can be shown that $\sigma_{\mathbf{e}_{aq}}^2 = 2^{-2B_a} \frac{4\pi^2}{12}$ [13]. In turn, we use the CRLB developed in [14] to define $\sigma_{\mathbf{e}_a}^2$ and, hence, $\sigma_{\mathbf{e}_a}^2 = \frac{4 \sin^2(\frac{\pi}{K}) \sigma_v^2}{NK\pi^2}$ where N is the number of samples using to estimate ϕ_s . Taking into account the aforementioned consideration, the practical M-DCB beamforming vector is now given by

$$\hat{\mathbf{w}}_M = \hat{\mu}_M \mathbf{\Lambda}^{-1} \hat{\mathbf{h}}_M, \quad (6)$$

where $\hat{\mu}_M = \left(\hat{\mathbf{h}}_M^H \mathbf{\Lambda}^{-1} \hat{\mathbf{h}}_M \right)^{-1}$.

3) *Bichromatic distributed CB (B-DCB)*: Exploiting the fact that for low AS a multi-ray channel -owing to a Taylor series expansion of its correlation matrix- can be properly approximated by two angular rays and hence considered as bichromatic, a bichromatic distributed CB (B-DCB) was recently proposed in [10] and [11]. Its beamforming vector is given by

$$\mathbf{w}_B = \mu_B \mathbf{\Lambda}^{-1} \mathbf{h}_B, \quad (7)$$

where $\mathbf{h}_B = \frac{1}{2} (\mathbf{a}(\sigma_\theta) + \mathbf{a}(-\sigma_\theta))$ and $\mu_B = \frac{2}{K} \left(1 + 2 \frac{J_1(\gamma(2\sigma_\theta))}{\gamma(2\sigma_\theta)} \right)^{-1}$. Note that in the conventional

scenario where the local scattering effect is neglected (i.e., $\sigma_\theta \rightarrow 0$) to assume monochromatic propagation channels, (7) is reduced to (5). It is also noteworthy that the B-DCB's implementation requires that the source estimates, quantizes and sends its direction ϕ_s and the AS σ_θ , thereby resulting in both estimation and quantization errors. The channel \mathbf{h}_B should be then substituted by $\hat{\mathbf{h}}_B = \mathbf{h}_B e^{-j(\mathbf{e}_a + \mathbf{e}_{aq} + \mathbf{e}_s + \mathbf{e}_{sq})}$ where \mathbf{e}_s and \mathbf{e}_{sq} are the AS estimation and quantization errors, respectively. Using the same approach as above, one can easily show for relatively small errors that $\hat{\mathbf{h}}_B = \mathbf{h}_B + \mathbf{e}_B$ where $\mathbf{e}_B = -j\mathbf{h}_B (\mathbf{e}_a + \mathbf{e}_{aq} + \mathbf{e}_s + \mathbf{e}_{sq})$ with variance $\sigma_{\mathbf{e}_B}^2 = \sigma_{\mathbf{e}_a}^2 + \sigma_{\mathbf{e}_{aq}}^2 + \sigma_{\mathbf{e}_s}^2 + \sigma_{\mathbf{e}_{sq}}^2$. Using a $(B_s + 1)$ -bit uniform quantization, it can be shown that $\sigma_{\mathbf{e}_{sq}}^2 = 2^{-2B_s} \frac{\pi^2}{12}$ [13]. Since AS estimation can be modeled as a DoA estimation of two point sources, we also use for simplicity the CRLB developed in [14] to define $\sigma_{\mathbf{e}_s}^2$ and, hence, $\sigma_{\mathbf{e}_s}^2 = \sigma_{\mathbf{e}_a}^2$. Therefore, the B-DCB beamforming weight is now

$$\hat{\mathbf{w}}_B = \hat{\mu}_B \mathbf{\Lambda}^{-1} \hat{\mathbf{h}}_B, \quad (8)$$

where $\hat{\mu}_B = \frac{2}{K} (1 + \sigma_{\mathbf{e}_B}^2)^{-1} \left(1 + 2 \frac{J_1(\gamma(2\sigma_\theta))}{\gamma(2\sigma_\theta)} \right)^{-1}$.

In the sequel, we will analyze and compare the performances of all the aforementioned CB designs.

IV. PERFORMANCE ANALYSIS IN TERMS OF ASANR

In this section, we analyze and compare the performance of the B-DCB against those of the M-DCB and OCB. Although being a revealing performance measure, the achieved SNR turns out to be a random quantity [3], [11]. This unfortunately hampers a rigorous analytical study of its behavior and properties. Hence, to analyze and compare the CB designs' performances, we introduce the following performance measure:

$$\tilde{\Upsilon}_*(\sigma_\theta) = \frac{\tilde{\xi}_{\tilde{\mathbf{w}}_*}}{\xi_{\tilde{\mathbf{w}}_B}}, \quad (9)$$

where $\tilde{\xi}_{\tilde{\mathbf{w}}} = \tilde{P}_{\tilde{\mathbf{w}}}(\phi_s) / \tilde{P}_{\tilde{\mathbf{w}},n}$ is the achieved average-signal-to-average-noise ratio (ASANR) when $\tilde{\mathbf{w}}$ is implemented with $\tilde{P}_{\tilde{\mathbf{w}}}(\phi_*) = \mathbb{E} \left\{ |\mathbf{w}^H \mathbf{h}|^2 \right\}$, called the average beampattern, and $\tilde{P}_{\tilde{\mathbf{w}},n} = \sigma_v^2 \mathbb{E} \left\{ \mathbf{w}^H \mathbf{\Lambda} \mathbf{w} \right\} + \sigma_n^2$ is the average noise power. In ideal conditions where all the estimation and quantization errors are negligible, we define the following performance measure:

$$\tilde{\Upsilon}_*^{\text{IDL}}(\sigma_\theta) = \frac{\tilde{\xi}_{\tilde{\mathbf{w}}_*}}{\xi_{\tilde{\mathbf{w}}_B}}, \quad (10)$$

Before comparing the beamformers' performances, we derive the expression of the ASANR $\tilde{\xi}_{\tilde{\mathbf{w}}_*}$ achieved using $\hat{\mathbf{w}}_*$. First, we have

$$\xi_{\tilde{\mathbf{w}}_*} = \frac{\mu_*^2 \| (\mathbf{h}_*^H + \mathbf{e}_*^H) \mathbf{\Lambda}^{-1} \mathbf{h} \|^2}{\sigma_v^2 \mu_*^2 (\mathbf{h}_*^H + \mathbf{e}_*^H) \mathbf{\Lambda}^{-1} (\mathbf{h}_* + \mathbf{e}_*) + \sigma_n^2 \left(\frac{\mu_*}{\hat{\mu}_*} \right)^2}. \quad (11)$$

Using the fact that \mathbf{h} and \mathbf{e}_* are statistically independent, $\tilde{\xi}_{\tilde{\mathbf{w}}_*}$ can then be expressed as

$$\tilde{\xi}_{\tilde{\mathbf{w}}_*} = \frac{\tilde{P}_{\tilde{\mathbf{w}}_*}(\phi_s) + \mathbb{E} \left\{ \mu_*^2 \| \mathbf{h}^H \mathbf{\Lambda}^{-1} \mathbf{e}_* \|^2 \right\}}{\tilde{P}_{\tilde{\mathbf{w}}_*,n}^r + \sigma_v^2 \mathbb{E} \left\{ \mu_*^2 \mathbf{e}_*^H \mathbf{\Lambda}^{-1} \mathbf{e}_* \right\} + \sigma_n^2 \left(\mathbb{E} \left\{ \left(\frac{\mu_*}{\hat{\mu}_*} \right)^2 \right\} - 1 \right)}. \quad (12)$$

Note that the each of the numerator and denominator decomposes into two terms corresponding to channel mismatch contribution (i.e., $\tilde{P}_{\mathbf{w}_*}(\phi_s)$ or $\tilde{P}_{\mathbf{w}_*,n}^r$, respectively) and channel quantization/estimation errors contribution (i.e., each remainder).

A. ASANR of B-DCB vs. OCB

In this section we carry out a comparison between the B-DCB and its OCB vis-a-vis. When the OCB technique is implemented in the network, it can be readily shown that $\tilde{P}_{\mathbf{w}_O,n} = \sigma_v^2 \mathbb{E} \left\{ \frac{1}{\|\mathbf{g}\|^2} \right\} + \sigma_n^2$ and $\tilde{P}_{\mathbf{w}_O}(\phi_*) = 1$. Let us introduce the following important theorem [15]:

Theorem 1: Assuming that α_l for $l = 1, \dots, L$ are Gaussian random variables, we have

$$\mathbb{E} \left\{ \frac{1}{\|\mathbf{g}\|^2} \right\} = \frac{L}{K(L-1)} \quad (13)$$

$$\mathbb{E} \left\{ \frac{1}{\|\mathbf{g}\|^4} \right\} = \frac{L^2}{K^2(L-1)(L-2)}. \quad (14)$$

Using (13), (14) and the results developed in [10] and [11], we obtain

$$\tilde{\Upsilon}_O(\sigma_\theta) = \tilde{\Upsilon}_O^{\text{IDL}}(\sigma_\theta) \frac{(1 + \sigma_{e_B}^2)^2}{1 + 2\frac{\sigma_{e_O}^2 L}{L-1} + \frac{\sigma_{e_O}^4 L^2}{(L-1)(L-2)}}, \quad (15)$$

where $\tilde{\Upsilon}_O^{\text{IDL}}(\sigma_\theta) = \frac{(1+2\frac{J_1(\gamma(2\sigma_\theta))}{4\Omega(0)})^2}{4\Omega(0)}$ with $\Omega(\phi) = \int p(\theta) \left(\frac{J_1(\gamma(\phi+\theta+\sigma_\theta))}{\gamma(\phi+\theta+\sigma_\theta)} + \frac{J_1(\gamma(\phi+\theta-\sigma_\theta))}{\gamma(\phi+\theta-\sigma_\theta)} \right)^2 d\theta$. Given the fact that when f_D increases $\sigma_{e_O}^2$ increases, it can be inferred from (15) that $\tilde{\Upsilon}_O(\sigma_\theta)$ decreases as expected. Moreover, it can be readily proven that $\tilde{\Upsilon}_O^{\text{IDL}}(0) = 1$. This is expected since, when there is no local scattering in the source vicinity (i.e., $\sigma_\theta = 0$), $\mathbf{w}_O = \mathbf{w}_B$. Simulations results in Section VI will also show that, in rural and suburban areas where σ_θ is small, $\tilde{\Upsilon}_O^{\text{IDL}}(\sigma_\theta) = 1$. Therefore, from (15), $\tilde{\Upsilon}_O(\sigma_\theta) < 1$ for large f_D and small AS. Consequently, the B-DCB is able to outperform its OCB vis-a-vis when σ_θ is small such as in rural and suburban areas. However, when σ_θ is relatively large such as in urban areas, one can easily show that $J_1(\gamma(2\sigma_\theta))/\gamma(2\sigma_\theta) \simeq 0$ [3] and, hence, it holds for large K that $\tilde{\Upsilon}_O^{\text{IDL}}(\sigma_\theta) \simeq (4\Omega(0))^{-1}$. Since $\Omega(0)$ decreases if σ_θ increases, $\tilde{\Upsilon}_O(\sigma_\theta)$ turns out to be a decreasing function of σ_θ for high AS. Consequently, in ideal conditions the OCB outperforms the B-DCB in terms of ASANR for high AS. However, it follows from (15) that this ASANR gain decreases if f_D increases. Simulations in Section VI will show that this results in a wider operational region in terms of AS values over which the B-DCB is favored against OCB.

B. ASANR of B-DCB vs. M-DCB

Using Theorem 1 and the results in [10] and [11], it can be shown for large K that

$$\tilde{\Upsilon}_M(\sigma_\theta) = \tilde{\Upsilon}_M^{\text{IDL}}(\sigma_\theta) \left(\frac{1 + \sigma_{e_B}^2}{1 + \sigma_{e_M}^2} \right)^2, \quad (16)$$

where $\tilde{\Upsilon}_M^{\text{IDL}}(\sigma_\theta) = \frac{\Gamma(0) \left(1 + 2\frac{J_1(\gamma(2\sigma_\theta))}{\gamma(2\sigma_\theta)} \right)^2}{4\Omega(0)}$ with $\Gamma(\phi) = \int p(\theta) \left(2\frac{J_1(\gamma(\phi+\theta))}{\gamma(\phi+\theta)} \right)^2 d\theta$. In [11], we proved that $\tilde{\Upsilon}_M^{\text{IDL}}(\sigma_\theta) \leq 1$ and the ASANR gain achieved using \mathbf{w}_B instead of \mathbf{w}_M can reach as much as 3 dB for high AS. However, from (16), $\tilde{\Upsilon}_M(\sigma_\theta) < \tilde{\Upsilon}_M^{\text{IDL}}(\sigma_\theta)$ only when $\sigma_{e_B}^2 > \sigma_{e_M}^2$ (i.e., small B_a and B_s). Therefore, the B-DCB always outperforms the M-DCB as found in ideal conditions, excluding exceptional circumstances of unrealistic low quantization levels (i.e., very large quantization errors) hard to justify in practice.

V. PERFORMANCE ANALYSIS IN TERMS OF LINK-LEVEL THROUGHPUT

The problem with the comparisons made above at ASANR level is that they do not factor in the different overhead costs incurred by each design. It is therefore appropriate to make comparisons in terms of the link-level throughput as well. Assuming without loss of generality a BPSK-modulated transmission, the link-level throughput achieved by $\hat{\mathbf{w}}_*$ is given by [16]

$$\mathcal{T}_{\hat{\mathbf{w}}_*}(\sigma_\theta) = 0.5 (R_T - R_{\hat{\mathbf{w}}_*}^{\text{oh}}) \mathbb{E} \{ \log_2(1 + \xi_{\hat{\mathbf{w}}_*}) \}, \quad (17)$$

where R_T and $R_{\hat{\mathbf{w}}_*}^{\text{oh}}$ are the transmission bit rate and the overhead bit rate allocated to $\hat{\mathbf{w}}_*$'s implementation. Obviously, $\mathcal{T}_{\hat{\mathbf{w}}_*}(\sigma_\theta)$ is intractable in closed-form which hampers its analytical study. However, the latter can be approximated as [15]

$$\mathcal{T}_{\hat{\mathbf{w}}_*}(\sigma_\theta) \simeq \tilde{\mathcal{T}}_{\hat{\mathbf{w}}_*}(\sigma_\theta) = 0.5 (R_T - R_{\hat{\mathbf{w}}_*}^{\text{oh}}) \log_2(1 + \tilde{\xi}_{\hat{\mathbf{w}}_*}). \quad (18)$$

Therefore, the throughput gain given by

$$\mathcal{G}_{\hat{\mathbf{w}}_*}(\sigma_\theta) = \frac{\tilde{\mathcal{T}}_{\hat{\mathbf{w}}_*}(\sigma_\theta) - \tilde{\mathcal{T}}_{\hat{\mathbf{w}}_B}(\sigma_\theta)}{\tilde{\mathcal{T}}_{\hat{\mathbf{w}}_B}(\sigma_\theta)}, \quad (19)$$

can be used to compare the CBs' performances. Yet we will shortly see below, both by analysis and simulations, that this simplifying assumption is still able to provide an analytical framework that is extremely insightful qualitatively.

A. Throughput of B-DCB vs. OCB

As discussed in Section III-1, OCB's implementation requires that the source broadcast all $[\mathbf{h}]_k, k = 1 \dots K$ for all K terminals. This process requires K time slots of B_c bits transmitted at an identification refreshment rate $f_{\text{IR}} = 1/T_{\text{IR}}$ where T_{IR} denotes the refreshment period. It is noteworthy that T_{IR} should satisfy $T_{\text{IR}} \geq T_c$ where $T_c = 0.423/f_D$ is the coherence time and f_D is the maximum Doppler frequency. For simplicity, we assume $f_{\text{IR}} = 2f_D$. Therefore, the OCB implementation overhead rate is $R_{\hat{\mathbf{w}}_O}^{\text{oh}} = 2KB_c f_D$ and, hence, its achieved throughput is

$$\tilde{\mathcal{T}}_{\hat{\mathbf{w}}_O}(\sigma_\theta) = 0.5 R_T (1 - 2KB_c \bar{f}_D) \log_2(1 + \tilde{\xi}_{\hat{\mathbf{w}}_O}). \quad (20)$$

As can be observed from (20), the achieved throughput using the OCB technique decreases if the number of terminals K increases. Furthermore, since when \bar{f}_D increases $\tilde{\xi}_{\hat{\mathbf{w}}_O}$ decreases, it follows then from the above result that $\tilde{\mathcal{T}}_{\hat{\mathbf{w}}_O}$ also

decreases if \bar{f}_D increases. Interestingly, from (20), B_c has two contradictory effects on $\tilde{\mathcal{T}}_{\hat{\mathbf{w}}_O}$. Indeed, if B_c increases the OCB overhead rate increases and, hence, $\tilde{\mathcal{T}}_{\hat{\mathbf{w}}_O}$ is decreased. However, as discussed above increasing B_c results in improves the ASANR $\tilde{\xi}_{\hat{\mathbf{w}}_O}$ and, therefore, the achieved throughput $\tilde{\mathcal{T}}_{\hat{\mathbf{w}}_O}$ is increased. The result in (20) could then be exploited to find the optimum number of quantization bits B_c^{opt} that maximizes the throughput achieved using the OCB technique.

On the other hand, the B-DCB implementation requires that the source estimates, quantizes and broadcasts ϕ_s and σ_θ . The angular estimate broadcasting requires only one time slot of B_a bits transmitted at a localization refreshment rate $f_{LR} = 1/T_{LR}$ where T_{LR} is the refreshment period. In turn, the AS estimate broadcasting requires one time slot of B_s bits transmitted at an estimation refreshment rate $f_{ER} = 1/T_{ER}$ where T_{ER} is the estimation refreshment period. Since T_{LR} and T_{ER} are typically very large compared to T_{IR} (i.e., $T_{LR} \gg T_{IR}$ and $T_{ER} \gg T_{IR}$), we have both f_{LR} and f_{ER} negligible compared to f_{IR} (i.e., $f_{LR} \simeq 0$ and $f_{ER} \simeq 0$), and hence we have $R_{\hat{\mathbf{w}}_B}^{\text{oh}} \simeq 0$. Therefore, the throughput achieved using the B-DCB is

$$\tilde{\mathcal{T}}_{\hat{\mathbf{w}}_B}(\sigma_\theta) \simeq 0.5R_T \log_2 \left(1 + \tilde{\xi}_{\hat{\mathbf{w}}_B} \right). \quad (21)$$

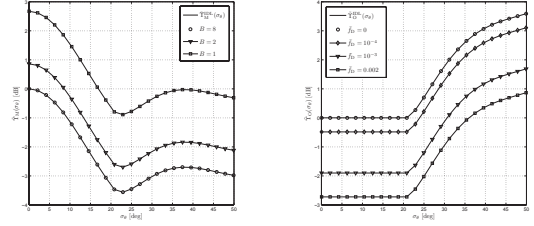
As can be shown from (21), in contrast with OCB, the B-DCB throughput is independent of the number of terminals K and the normalized Doppler frequency \bar{f}_D and, therefore, $\mathcal{G}_{\hat{\mathbf{w}}_O}(\sigma_\theta)$ decreases if K and/or \bar{f}_D increases. Furthermore, since we showed in Section IV-A that $\tilde{\xi}_{\hat{\mathbf{w}}_B} \geq \tilde{\xi}_{\hat{\mathbf{w}}_O}$ for high SNR and relatively large B_a and B_s , we have $\mathcal{G}_{\hat{\mathbf{w}}_O}(\sigma_\theta) < 0$ for large K and low AS. Consequently, the B-DCB outperforms, in rural and suburban areas, its OCB vis-a-vis in terms of achieved throughput. Simulations in Section VI will show that this results in a wider operational region in terms of AS values over which the B-DCB is favored against OCB. They will also establish that this operation region increases with K and \bar{f}_D and reaches as much as 40 deg for large K and high \bar{f}_D , against about 17 deg in ideal conditions (i.e, without accounting for any overhead cost or any quantization or estimation error). This further proves the efficiency the B-DCB technique.

B. Throughput of B-DCB vs. M-DCB

As discussed in Section III-2, the M-DCB implementation only requires that the source estimates, quantizes and broadcasts its angle ϕ_s . Following similar steps as above, it can be easily shown that $R_{\hat{\mathbf{w}}_M}^{\text{oh}} \simeq 0$ and, therefore, $\tilde{\mathcal{T}}_{\hat{\mathbf{w}}_M}(\sigma_\theta) \simeq 0.5R_T \log_2 \left(1 + \tilde{\xi}_{\hat{\mathbf{w}}_M} \right)$. Thus, we obtain

$$\mathcal{G}_{\hat{\mathbf{w}}_M}(\sigma_\theta) \simeq \frac{\log_2 \left(1 + \tilde{\xi}_{\hat{\mathbf{w}}_M} \right)}{\log_2 \left(1 + \tilde{\xi}_{\hat{\mathbf{w}}_B} \right)} - 1. \quad (22)$$

Since for reasonable B_s and B_a $\tilde{\xi}_{\hat{\mathbf{w}}_M} \leq \tilde{\xi}_{\hat{\mathbf{w}}_B}$, we have $\mathcal{G}_{\hat{\mathbf{w}}_M}(\sigma_\theta) \leq 0$, it follows from (22) that the B-DCB is always more efficient than the M-DCB in terms of achieved throughput.



(a) $\tilde{\mathcal{Y}}_M^{\text{IDL}}(\sigma_\theta)$ and $\tilde{\mathcal{Y}}_M(\sigma_\theta)$ for (b) $\tilde{\mathcal{Y}}_O^{\text{IDL}}(\sigma_\theta)$ and $\tilde{\mathcal{Y}}_O(\sigma_\theta)$ for different values of B . $B = 8$ and different values of \bar{f}_D .

Fig. 2. ASANR comparison for $K = 20$ and $B = B_a = B_s = B_c$.

VI. SIMULATION RESULTS

Numerical experiments are performed to verify the analytical results. In all examples, we assume that the noises' powers σ_n^2 and σ_v^2 are 10 dB below the source transmit power. It is also assumed that ϕ_s and σ_θ are estimated using $N = 10$ samples. Furthermore, we assume that the number of rays is $L = 6$ and that their phases are uniformly distributed. All the results are obtained by averaging over 10^6 random realizations of r_k , ψ_k , $[\mathbf{f}]_k$ for $k = 1, \dots, K$ and α_l , θ_l for $l = 1, \dots, L$ as well as all the estimation and quantization errors.

Fig. 2(a) displays $\tilde{\mathcal{Y}}_M^{\text{IDL}}(\sigma_\theta)$ and $\tilde{\mathcal{Y}}_M(\sigma_\theta)$ for different values of $B = B_a = B_s$. As can be observed from this figure, for practical value $B = 8$, $\tilde{\mathcal{Y}}_M(\sigma_\theta) \simeq \tilde{\mathcal{Y}}_M^{\text{IDL}}(\sigma_\theta)$. This is expected since for high quantization levels quantization errors are negligible. In such a case, we also show that the B-DCB is much more efficient in terms of achieved ASANR than its M-DCB vis-a-vis. However, from Fig. 2, the achieved ASANR gain using $\hat{\mathbf{w}}_B$ instead of $\hat{\mathbf{w}}_M$ decreases with B . This is expected since $\tilde{\xi}_{\hat{\mathbf{w}}_B}$ is affected by both quantization errors \mathbf{e}_{aq} and \mathbf{e}_{sq} while $\tilde{\xi}_{\hat{\mathbf{w}}_M}$ involves only \mathbf{e}_{aq} . Furthermore, it follows from this figure that the M-DCB outperforms the B-DCB only for unrealistic low quantization levels which are hard to justify in practice. This corroborates the discussion made in Section IV-B.

Fig. 2(b) plots $\tilde{\mathcal{Y}}_O(\sigma_\theta)$ for $B = B_a = B_s = B_c = 8$ and different values of \bar{f}_D . From this figure, for low AS the B-DCB always outperforms the OCB design even for small \bar{f}_D . Furthermore, Fig. 2(b) establishes that the achieved ASANR gain using $\hat{\mathbf{w}}_O$ instead of $\hat{\mathbf{w}}_B$ decreases when \bar{f}_D increases. This corroborates the discussion made in Section IV-A.

Figs. 3(a) and 3(b) plot $\mathcal{G}_{\hat{\mathbf{w}}_O}(\sigma_\theta)$ for different values of \bar{f}_D and B_c . They also plot $\mathcal{G}_{\hat{\mathbf{w}}_O}(\sigma_\theta)$ in ideal conditions (i.e, without accounting for any overhead cost or any quantization or estimation error). As can be observed from these figures, in rural and suburban areas where the AS is relatively low, the B-DCB always outperforms the OCB in terms of achieved throughput. Their performances become actually equal only in idealistic conditions that ignore the practical effects of both overhead and estimation and quantization errors. Figs. 3(a) and 3(b) also confirm and illustrate the existence of an optimum quantization level B_c^{opt} that maximizes the throughput (i.e.,

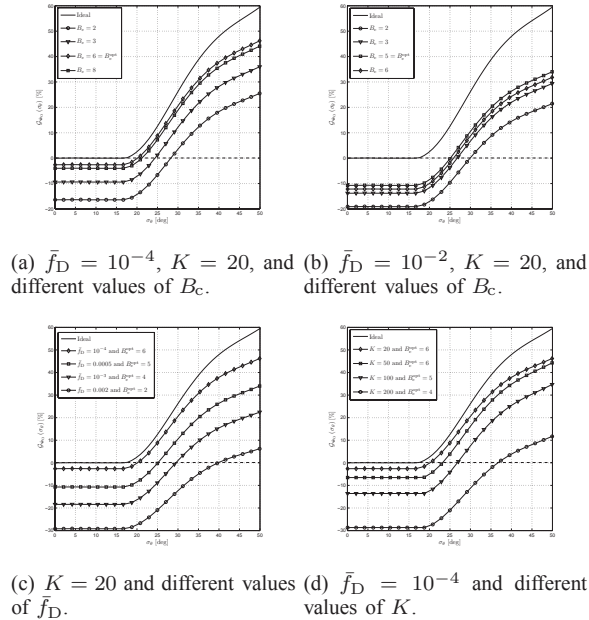


Fig. 3. Throughput-level comparison.

level that best minimizes combined losses due to errors and overhead) found to be equal to 6 and 5 at \bar{f}_D set to 10^{-4} and 10^{-2} , respectively. At these optimum quantization levels, OCB suffers from throughput losses against B-DCB of about 3% and 10%, respectively. The B-DCB's throughput gains against OCB indeed increase with higher normalized Doppler frequencies. The operational region in terms of AS values over which the B-DCB is favored against OCB also increases from a nominal low AS range of about 17 deg in ideal conditions to about 20 and 25 deg, respectively.

Figs. 3(c) and 3(d) plot $\mathcal{G}_{\hat{w}_o}(\sigma_\theta)$ for different values of \bar{f}_D and K , respectively. In these figures, curves are plotted after performing a numerical evaluation of the optimum quantization level B_c^{opt} for each value of \bar{f}_D and K . For instance, we find that $B_c^{\text{opt}} = 2$ bits when $\bar{f}_D = 0.002$ and $K = 20$ while $B_c^{\text{opt}} = 4$ bits when $\bar{f}_D = 10^{-4}$ and $K = 200$. As can be seen from these figures, the B-DCB's throughput gain against OCB increases if \bar{f}_D increases and/or K increases. Furthermore, the B-DCB operational region also increases if \bar{f}_D and/or K increases and can reach as much as 40 deg when $\bar{f}_D = 0.002$ and $K = 20$. All these observations corroborate all the elements of our discussion in Section V-A.

VII. CONCLUSION

In this work, we considered the M-DCB and the B-DCB as well as the optimal CSI-based CB (OCB) design to achieve a dual-hop communication from a source to a receiver, through a wireless network comprised of K independent terminals. Assuming the presence of local scattering in the source vicinity and accounting for estimation and quantization errors incurred by each CB design, we performed an ASANR comparison between all CB designs and derived their true achieved ASANR in closed-form. For low AS, where both designs nominally achieve the same ASANR in ideal conditions, we showed that

the B-DCB always outperforms OCB, more so and at larger regions of AS values when errors increase. Excluding exceptional circumstances of unrealistic low quantization levels (i.e., very large quantization errors) hard to justify in practice, we also showed that the new B-DCB always outperforms the M-DCB as recently found nominally in ideal conditions. This work is also the first to push the performance analysis of CB to the throughput level by taking into account the feedback overhead cost incurred by each design. We proved both by concordant analysis and simulations that the B-DCB is able to outperform, even for high AS values, the OCB which is penalized by its prohibitive implementation overhead, especially for a large number of K and/or \bar{f}_D . Indeed, it was shown that the operational regions in terms of AS values over which the new B-DCB is favored against OCB in terms of achieved throughput can reach up to 40 deg.

REFERENCES

- [1] H. Ochiai, P. Mitran, H. V. Poor, and V. Tarokh, "Collaborative beamforming for distributed wireless ad hoc sensor networks," *IEEE Trans. Signal Process.*, vol. 53, pp. 4110-4124, Nov. 2005.
- [2] K. Zarifi, A. Ghayeb, and S. Affes, "Distributed beamforming for wireless sensor networks with improved graph connectivity and energy efficiency," *IEEE Trans. Signal Process.*, vol. 58, pp. 1904-1921, Mar. 2010.
- [3] K. Zarifi, S. Zaidi, S. Affes, and A. Ghayeb, "A distributed amplify-and-forward beamforming technique in wireless sensor networks," *IEEE Trans. Signal Process.*, vol. 59, pp. 3657-3674, Aug. 2011.
- [4] K. Zarifi, S. Affes, and A. Ghayeb, "Collaborative null-steering beamforming for uniformly distributed wireless sensor networks," *IEEE Trans. Signal Process.*, vol. 58, pp. 1889-1903, Mar. 2010.
- [5] M. Bengtsson and B. Ottersten, "Low-complexity estimators for distributed sources," *IEEE Trans. Signal Process.*, vol. 48, pp. 2185-2194, Aug. 2000.
- [6] A. Amar, "The effect of local scattering on the gain and beamwidth of a collaborative beamforming for wireless sensor networks," *IEEE Trans. Wireless Commun.*, vol. 9, pp. 2730-2736, Sep. 2010.
- [7] M. Souden, S. Affes, and J. Benesty, "A two-stage approach to estimate the angles of arrival and the angular spreads of locally scattered sources," *IEEE Trans. Signal Process.*, vol. 56, pp. 1968-1983, May 2008.
- [8] Y. Jing and H. Jafarkhani, "Network beamforming using relays with perfect channel information," *IEEE Trans. Inf. Theory*, vol. 55, pp. 2499-2517, June 2009.
- [9] Y. Zhao, R. Adve, and T. Lim, "Improving amplify-and-forward relay networks: Optimal power allocation versus selection," *IEEE Trans. Wireless Commun.*, vol. 6, pp. 3114-3123, Aug. 2007.
- [10] S. Zaidi and S. Affes, "Distributed beamforming for wireless sensor networks in local scattering environments" *Proc. IEEE VTC'2012-Fall*, Québec City, Canada, Sep. 3-6, 2012.
- [11] S. Zaidi and S. Affes, "Distributed collaborative beamforming in presence of local scattering," submitted to *IEEE Trans. Signal Process.*
- [12] S. Affes and P. Mermelstein, "Adaptive space-time Processing for wireless CDMA," Chap. 10, pp. 283-321, in *Adaptive Signal Processing: Application to Real-World Problems*, J. Benesty and A. H. Huang, Eds., Springer, Berlin, Germany, Feb. 2003.
- [13] A. V. Oppenheim, R. W. Schaffer, and J. R. Buck, *Discrete-Time Signal Processing*, 2nd edition Prentice Hall, New Jersey, USA, 1999.
- [14] F. Bellili, S. B. Hassen, S. Affes, and A. Stephenne, "Cramer-Rao lower bounds of DOA estimates from square QAM-modulated signals," *IEEE Trans. Signal Process.*, vol. 59, pp. 1675-1685, June 2011.
- [15] S. Zaidi and S. Affes, "SNR and throughput analysis of distributed collaborative beamforming in locally-scattered environments," Invited Paper, *Wiley Journal of Wireless Commun. and Mobile Computing*, vol. 12, pp. 1620-1633, 2012.
- [16] M. K. Simon and M.-S. Alouini, *Digital Communications over Fading Channels*, Wiley, New York, USA, 2000.